



## Research Article

# Effect of Reinforcement Ratio and Particle Size on the Physical and Mechanical Performance of Epoxy Matrix Panels and Waste Wood from Iroko *Chlorophora excelsa* from Cameroon

Claude Takoumbe <sup>1,2,3</sup>, Joseph Zobo Mfomo <sup>4</sup>, Achille Bernard Biwolé,<sup>4</sup>  
Elvis Mbou Tiaya,<sup>1,2</sup> Jean Aimé Mono,<sup>5,6</sup> Prince Hermann Pokem Nguimjeu,<sup>1,2</sup>  
and Linus Ntsotsa Biwolé<sup>4</sup>

<sup>1</sup>Department of Mechanical Engineering, ENSET, University of Douala, P.O. Box: 1872, Douala, Cameroon

<sup>2</sup>Mechanical Laboratory (LM), Doctoral Training Unit in Engineering Sciences (UFD-SI), University of Douala, P.O. Box: 1872, Douala, Cameroon

<sup>3</sup>Laboratory of Mechanic and Adapted Materials Laboratory (LAMMA), ENSET–University of Douala, Douala, Cameroon

<sup>4</sup>Laboratory of Forest Resources and Wood Valorization, ENSET, University of Douala, P.O. Box: 1872, Douala, Cameroon

<sup>5</sup>Basic Science Department, Advanced Technical Teacher Training School University of Douala, Douala, Cameroon

<sup>6</sup>Textile and Clothing Industries Department, ENSET University of Douala, P.O. Box: 1872, Douala, Cameroon

Correspondence should be addressed to Claude Takoumbe; takoumceleste@yahoo.fr and Joseph Zobo Mfomo; zobo\_mfomo@yahoo.fr

Received 30 January 2024; Revised 12 March 2024; Accepted 4 April 2024; Published 23 April 2024

Academic Editor: Ivan Giorgio

Copyright © 2024 Claude Takoumbe et al. This is an open access article distributed under the Creative Commons Attribution License, which permits unrestricted use, distribution, and reproduction in any medium, provided the original work is properly cited.

The use of local materials developed from natural reinforcements remains a major challenge for many researchers in the development of the industry and the fight against pollution. The wood industry generates large quantities of environmental waste, including Iroko wood. To give Iroko a second life, this study uses Iroko sawdust waste to make an epoxy matrix composite material. The composite was produced using a cold pressing technique based on moving the top and bottom plates to a thickness of 10 mm. On this basis, three particle sizes [ $t < 0.35$ ], [0.35–0.63], and [0.63–1] were used, as well as three reinforcement ( $R$ )/matrix ( $M$ ) percentages of 50R/50M, 60R/40M, and 70R/30M, where  $R$  is the reinforcement percentage and  $M$  is the matrix percentage. The physical tests, apparent and real density, porosity, moisture content, water absorption rate, absorption and desorption kinetics, diffusion theory, and activation energy were determined by the gravimetric method. A three-point bending test was carried out in accordance with the ASTM D790 for mechanical tests. The results show that the addition of Iroko particles lightens the material by reducing its density. The hydrophilic nature of Iroko particles increases the absorption rate and porosity, with good diffusion capacity as the particle size and percentage increase. The material produced can be light and porous, with possible applications in thermal insulation. In terms of kinetics, Verma et al.'s model best correlates the experimental desorption points for the 3 isotherms, while Page's model best correlates the water absorption points. The mechanical results show that Young's modulus and stress at break decrease with an increase in the reinforcement percentage and particle size. The mechanical results can be used to define the material's applications in construction and furniture. In accordance with the EN312 standard, the composites produced can be classified as type 2 lightweight materials, suitable for use in dry and damp areas.

## 1. Introduction

The industrial world is becoming increasingly involved in the fight against pollution by developing materials derived

from natural resources, with the aim of replacing synthetic materials. These synthetic materials are very expensive, dense, and polluting, releasing greenhouse gases into the environment [1, 2]. Nature itself abounds in a variety of

natural materials, including fibres, wood, and straw. These exploited or underexploited resources available in nature can contribute to the production of various materials useful to the public [3–6]. These natural resources can be used as reinforcement with thermosetting or thermoplastic matrices in the development of composites [1, 7]. Several parameters can influence material properties, including the nature of the reinforcement or matrix, particle size, molding technique, and test equipment. This justifies the variability of results for a material. With an increasing demand for composites developed from natural resources [4, 8], it is necessary to exploit these resources to develop new materials.

Today, many of these resources are recycled and used in the manufacture of materials for thermal insulation, furniture, construction, civil engineering, and the automotive industry [1, 9]. The use of tropical woods generates a number of waste products that contribute to the development of diseases (asthma, cough, chronic bronchitis and, more rarely, pulmonary fibrosis, or allergic alveolitis) to the occupation of space and to environmental pollution during the various processing phases [10, 11]. Unfortunately, despite the fact that a considerable volume of wood is exploited each year in Cameroon, barely 30–36% is processed [11–13]. This is due to the low efficiency of the wood processing industry. Around 64–70% of wood ends up as residues in sawmills, and only 10% of sawmill residues are recovered [11, 14]. It is essential to develop new materials from this waste, of which there is an abundant supply. Iroko, whose scientific name is *Chlorophora excelsa*, has been the subject of several studies in Cameroon, and its waste has been used as reinforcement in the manufacture of bricks for construction and thermal insulation applications [11, 15, 16]. Other studies have shown that Iroko has a density of  $600 \text{ kg}\cdot\text{m}^{-3}$  [11, 17] and that it can be used in both dry and damp environments as construction and thermal insulation timber [16, 18]. According to the work of Cunha et al. [15], Iroko has a ductile behavior, a modulus of elasticity of 9.95 GPa, and a mechanical strength of 105.3 MPa. The work of Papy et al. [19] has shown that this waste can be used to reinforce concrete. It has been shown that when the percentage of Iroko waste increases, the concrete densifies less and its absorption content increases. Young's modulus, flexural, tensile, and compressive strengths also decrease. Cameroonian Iroko *Chlorophora excelsa* is currently attracting a great deal of interest in the literature. To the authors' knowledge, no studies on the characterisation of composites reinforced with Iroko particles and thermosetting or thermoplastic matrices have been documented in the literature. The residues resulting from the processing of these tropical species were chosen because of their availability, their energy potential, and the environmental problems posed by sawdust during its processing cycle [11, 20, 21]. Indeed, Iroko is one of the 5 most locally exploited roundwood species in Cameroon [22]. With production estimated at  $487,415 \text{ m}^3$ , this species represents around 4% of the total wood production in Cameroon [22].

This study focuses on the recycling of Iroko *Chlorophora excelsa* wood waste from Cameroon in the production of composites for possible applications in furniture,

construction, filling, and thermal insulation. Physical tests (density, porosity, absorption, and diffusion theory) and mechanical tests will be used to determine the characteristics of the composite produced.

## 2. Materials and Methods

The Iroko particles used to produce the composites in this study came from a wood-processing industry located at Ndogbong in Douala District 5 in the Littoral region of Cameroon. A set of three sieves was used to distinguish particle sizes. The choice of the sieve sizes was based on the works of Bouafif et al. [23] and Migneault et al. [24]. The epoxy matrix was purchased from a supermarket in the Littoral region. Figure 1 illustrates the steps involved in obtaining the particles. In this process, Figure 1(a) shows the Iroko waste, Figure 1(b) shows the sieving, and Figure 1(c) shows the particle sizes obtained.

The mass of the different particle sizes (Figure 2(a)) was determined using a digital balance with an accuracy of 0.01 g. The mass of the epoxy resin was also determined (Figure 2(b)). The particles and epoxy resin were manually homogenized for 10 minutes (Figure 2(c)) to ensure good wettability, in accordance with the formulation plan in Table 1, before being introduced into a 4 compartment mold (Figure 2(d)). The mold was covered with a cling film to prevent sticking during curing. The compaction system was based on moving the upper and lower plates until they reached the end of their stroke, as described by Mbou et al. [1]. The molded samples were left in the mold to cure for 24 hours. Figure 2(e) shows the composites produced in the mold, and Figure 2(f) shows some samples of the molded composites. The composites obtained measured  $180 * 180 * 10 \text{ mm}$ . Figure 2 shows the molded composites.

Table 1 illustrates the different codes used. In Table 1, the 50/50, 60/40, and 70/30 formulations correspond to 50%, 60%, and 70% reinforcement and 50%, 40%, and 30% matrix, respectively, for all the particle sizes used. The different mass fractions were calculated using the following relationship:

$$\begin{cases} m_p = \frac{\rho_p}{\rho_p \vartheta_p + \rho_m (1 - \vartheta_p)} \vartheta_p, \\ m_m = \frac{\rho_m}{\rho_p \vartheta_p + \rho_m (1 - \vartheta_p)} \vartheta_m, \end{cases} \quad (1)$$

where  $\vartheta_m$  is the matrix volume fraction;  $\vartheta_p$  is the particle volume fraction;  $\rho_m$  is the matrix density;  $\rho_p$  is the particle density. The density of the matrix (epoxy) is  $1200 \text{ kg}/\text{m}^3$  [4], and that of the reinforcement (Iroko) is  $600 \text{ kg}\cdot\text{m}^{-3}$  [11].

### 2.1. Physical Characterisations of the Composite

**2.1.1. Determination of Drying Parameters.** Drying was carried out using a gravimetric method, with a mass setting cycle repeated at regular time intervals until a constant mass was obtained [25]. The constant mass was obtained after 200 minutes. Based on the literature [26], 3 isotherms at  $70^\circ\text{C}$ ,  $80^\circ\text{C}$ , and  $90^\circ\text{C}$  were used. 5 samples of  $50 * 10 * 4 \text{ mm}$



FIGURE 1: Particle size distinction: (a) supply; (b) sieving; and (c) different particle sizes.

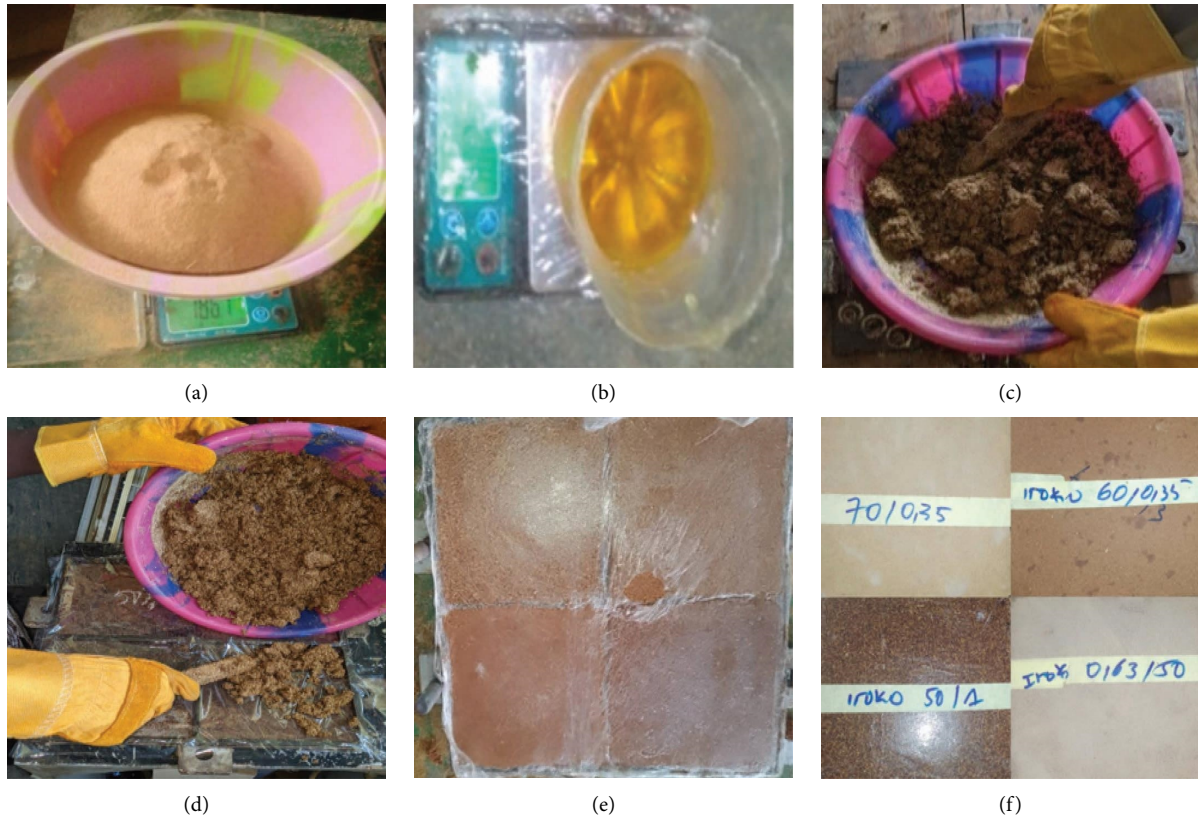


FIGURE 2: Molding process: (a) weighing particles; (b) weighing the epoxy matrix; (c) homogenization of particles and resin; (d) tamping in the mold; (e) composite in the mold; and (f) composite obtained.

TABLE 1: Formulation code.

	Reinforcement rate			
	50R-50M	60R-40M	70R-30M	
Particle size	[t < 0.35]	50/50	60/40	70/30
	[0.35-0.63]	50/50	60/40	70/30
	[0.63-1]	50/50	60/40	70/30

were used per isotherm for a total of 135 samples. The geometry of the samples was measured using a 1/50 digital calliper, and the mass of the samples was measured using a 0.01g precision digital balance. The degree of hygroscopicity (relative humidity (THR%)) was determined from the following equation:

$$THR (\%) = \left( \frac{m_h}{m_s} - 1 \right) * 100, \quad (2)$$

where THR (%) is the moisture content;  $m_h$  is the mass of the sample in the humid state (g);  $m_s$  is the mass of the sample in the anhydrous state (g). To describe the drying kinetics, the mass loss rate (MR), a unitless value, is calculated by equation (3). In this relationship,  $m_t$  represents the mass at each instant.

$$MR = \frac{m_t - m_s}{m_h - m_s}. \quad (3)$$

To better express the drying process, models of the drying kinetics were identified in the literature to correlate

the experimental points. These models are presented in Table 2 along with the number of parameters for each model.

The empirical model will be chosen on the basis of its high correlation with the experimental points close to 1 ( $R^2$ ), the lowest root mean square error (RMSE), and the smallest model parameters. Assuming that diffusion occurs in the thickness direction, the diffusion coefficient was calculated using equation (4) and the diffusion was corrected using equation (5). This approach in determining diffusion has been used by Scida et al. [27] on other composites.

$$D_{\text{eff}} = \left( \frac{4 * K_{\text{ABS}} * e^2}{\pi^2} \right), \quad (4)$$

$$D_{\text{Ceff}} = D_{\text{eff}} * \left( 1 + \frac{e}{L} + \frac{e}{l} \right)^{-2}, \quad (5)$$

where  $D_{\text{Ceff}}$  is the corrected diffusion coefficient;  $L$  is the length of the sample (m);  $l$  is the width of the sample in (m);  $e$  is the thickness of the sample along the diffusion axis. The  $K_{\text{ABS}}$  coefficient is the slope of the linear part obtained experimentally according to works from the literature [28, 29]. In this equation, the slope of  $K_{\text{ABS}}$  is determined by the function  $\ln(MR) = f(t)$ . The activation energy was determined using the following Arrhenius equation:

$$D_{\text{eff}} = D_0 \exp\left(-\frac{E_a}{RT}\right), \quad (6)$$

where  $R$  is the perfect gas constant (8.314 J/mol<sup>o</sup>K);  $T$  is the absolute temperature of the drying chamber in Kelvin (°K);  $D_0$  is the Arrhenius constant in m<sup>2</sup>/s;  $E_a$  is the activation energy in kJ/mol. The logarithmic transformation of equation (6) gives the following equation:

$$\ln(D_{\text{eff}}) = \ln(D_0) - \left(\frac{E_a}{R}\right) * \left(\frac{1}{T}\right). \quad (7)$$

The values of  $D_{\text{eff}}$  calculated for the different experiments are plotted as a function of  $1/T$  where the slope of the straight line is defined by equation (8) with  $E_a$  defined by equation (9).

$$D = \frac{a}{T} + b, \quad (8)$$

$$E_a = a * R. \quad (9)$$

**2.1.2. Determination of Apparent Density, True Density, and Porosity.** Bulk density was determined using the gravimetric method following the protocol in the ISO 1183-1: 2012 standard [2]. 9 samples of 20 \* 20 \* 10 mm previously dried at 105°C for 3 hours were tested by formulation with a total of 81 samples. The geometry of the samples was measured using a digital calliper with an accuracy of 1/50, and the dry mass was measured using a digital balance with an accuracy of 0.01 g. The relationship in (10) was used to calculate the bulk density.

$$\rho_a (\text{kg.m}^{-3}) = \left( \frac{M_s}{V_s} \right), \quad (10)$$

where  $\rho_a$  is the bulk density (kg.m<sup>-3</sup>);  $M_s$  is the dry mass of samples (kg);  $V_s$  is the dry volume of the samples (m<sup>3</sup>).

The real density is calculated using the gravimetric method based on the displacement of the water column in accordance with works from the literature [3, 4, 30]. Real density was calculated using the following equation:

$$\rho_R (\text{kg.m}^{-3}) = \left( \frac{M}{V_R} \right), \quad (11)$$

where  $\rho_R$  is the real density (kg.m<sup>-3</sup>); sample mass (kg);  $V_R$  is the real sample volume (m<sup>3</sup>).

The porosity rate was calculated using the relationship in (12) in accordance with the ISO 5017 standard [3].

$$P (\%) = \left( 1 - \frac{\rho_a}{\rho_R} \right) * 100. \quad (12)$$

### 2.1.3. Determination of Water Absorption Parameters.

The study of water absorption was carried out using the gravimetric method with discontinuous weighing of the mass as described by Takoumbe et al. [2] and Mbou et al. [31]. The samples had the same characteristics as those used for drying. 5 samples per formulation with a total of 45 were immersed in distilled water at 28°C following a discontinuous weighing cycle until saturation. The saturation time is observed when the mass becomes constant. For this work, saturation was observed after 1440 min. The absorption rate was determined from equation (13), while the ratio was determined from equation (14) [9, 32].

$$W (\%) = \left( \frac{M_f}{M_i} - 1 \right) * 100, \quad (13)$$

$$MR = \frac{M_t - M_i}{M_f - M_i}, \quad (14)$$

where  $M_f$  is the mass of the sample saturated with water (g);  $M_i$  is the mass of the sample in the anhydrous state (g);  $M_t$  is the mass of the sample at the time of analysis (g). Several water absorption models (Table 3) have been identified in the literature to correlate experimental points.

The empirical model is chosen using the same parameters for drying. Absorption diffusion, which is in the same direction as drying, was calculated by equation (4). The corrected diffusion is calculated using equation (5). In this equation, the slope of  $K_{\text{ABS}}$  is determined from the function  $\ln(1 - MR) = g(t)$  [26].

### 2.2. Mechanical Characterisation by Three-Point Bending Test.

The bending test was carried out in accordance with the ASTM D790 standard [2]. The specimens had dimensions of 150 \* 15 \* 7 mm and were subjected to a load of 5 kN at a rate of 5 mm.min<sup>-1</sup>. Figure 3 shows the stages of the tensile test. In these stages, Figure 3(a) shows the specimens for this purpose, Figure 3(b) shows a specimen setup on the test device, and Figure 3(c) shows some specimens after testing.

TABLE 2: Models used for drying kinetics.

Authors	Mathematical models	Parameters	References
Peleg	$f(t) = 1 - [t / (a + b * t)]$	02	
Page	$f(t) = \exp(-k * \hat{t}n)$	02	[25, 26]
Verma et al.	$f(t) = a * \exp(-k * t) + (1 - a) * \exp(-g * t)$	04	
Anderson et Pabis	$f(t) = a * \exp(-k * t) + b * \exp(-g * t) + c * \exp(-h * t)$	06	

$a, b, g, k, h,$  and  $n$  represent model parameters;  $t$  represents drying time (minutes).

TABLE 3: Different mathematical models.

Authors	Mathematical models	Parameters	References
Page	$g(t) = 1 - a * \exp(-k * \hat{t}n)$	03	
Mohsenin	$g(t) = a * [1 - \exp(-k * t)] + c * d * t$	04	[2, 31]
Sikame	$g(t) = c - a * \exp(-k * t) - b * \exp(-m * t)$	05	

$a, b, c, k, m,$  and  $n$  represent model parameters;  $t$  represents absorption time (minute).

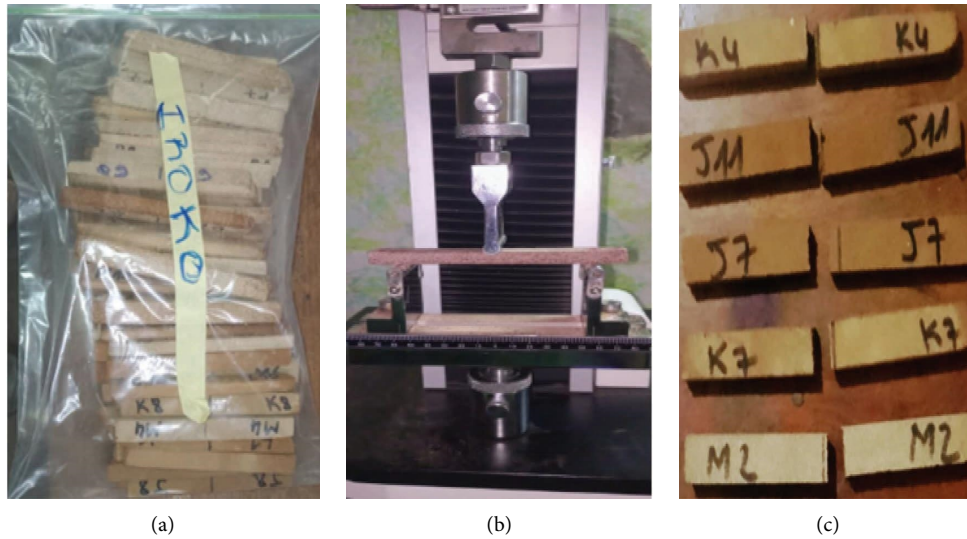


FIGURE 3: Three-point bending test: (a) samples to be tested; (b) sample being tested; and (c) sample already tested.

The bending parameters, in particular Young's modulus, were calculated using equation (15) while the stress at rupture was calculated using equation (16).

$$E_f = K * \frac{L^3}{48 * I_{GZ}}, \quad (15)$$

$$\sigma_{Rf} = \frac{3 * F * L}{2 * b * h^2}, \quad (16)$$

where  $E_f$  is Young's modulus in bending (MPa);  $\sigma_{Rf}$  is the stress at break;  $K$  is the slope of the linear part determined using equation (17);  $L$  is the useful length of the sample (mm);  $I_{GZ}$  is the moment of inertia calculated from equation (equation (18));  $b$  is the breadth of the sample (mm);  $f$  is the displacement at break (mm);  $h$  is the height of the sample (mm);  $\Delta F$  is the variation in the load applied until failure (N);  $\Delta f$  is the variation in displacement (mm).

$$K = \frac{\Delta F}{\Delta f}, \quad (17)$$

$$I_{GZ} = \frac{bh^3}{12}, \quad (18)$$

where  $\Delta F$  is the variation in the load applied until failure (N);  $\Delta f$  is the variation in displacement (mm).

### 3. Results and Discussion

#### 3.1. Physical Characteristics

**3.1.1. Drying Study.** In this study, the drying kinetics model was chosen on the basis of its highest  $R^2$  correlation coefficient, lowest root-mean-square error (RMSE), and smallest parameters. These parameters are presented in Table 4 for all formulations and isotherms.

TABLE 4: Correlation coefficients and root mean square error for composites.

Authors	Different formulations	$R^2$			RMSE			
		90°C	80°C	70°C	90°C	80°C	70°C	
Peleg	[ $t < 0.35$ ]	50/50	0.989	0.998	0.991	0.042	0.020	0.036
		60/40	0.995	0.993	0.995	0.029	0.034	0.026
		70/30	0.999	0.991	0.989	0.013	0.039	0.038
	[0.35–0.63]	50/50	0.997	0.994	0.995	0.020	0.031	0.025
		60/40	0.993	0.993	0.980	0.035	0.035	0.054
		70/30	0.998	0.997	0.991	0.019	0.023	0.036
	[0.63–]	50/50	0.971	0.995	0.988	0.058	0.029	0.040
		60/40	0.993	0.998	0.991	0.034	0.020	0.036
		70/30	0.998	0.993	0.989	0.016	0.035	0.038
Page	[ $t < 0.35$ ]	50/50	0.996	0.997	0.990	0.027	0.022	0.038
		60/40	0.997	0.995	0.992	0.023	0.030	0.033
		70/30	0.999	0.993	0.992	0.014	0.035	0.034
	[0.35–0.63]	50/50	0.999	0.994	0.998	0.010	0.031	0.018
		60/40	0.997	0.995	0.988	0.020	0.028	0.041
		70/30	0.998	0.998	0.990	0.018	0.020	0.038
	[0.63–1]	50/50	0.977	0.994	0.994	0.052	0.030	0.029
		60/40	0.998	0.997	0.991	0.018	0.023	0.035
		70/30	0.997	0.997	0.988	0.021	0.022	0.041
Verma et al.	[ $t < 0.35$ ]	50/50	0.999	0.998	0.986	0.004	0.019	0.041
		60/40	0.999	0.996	0.997	0.012	0.030	0.024
		70/30	0.999	0.994	0.997	0.006	0.033	0.023
	[0.35–0.63]	50/50	0.999	0.996	0.999	0.004	0.025	0.007
		60/40	0.999	0.996	0.992	0.006	0.029	0.037
		70/30	0.999	0.998	0.995	0.014	0.019	0.028
	[0.63–1]	50/50	0.979	0.996	0.997	0.054	0.028	0.022
		60/40	0.999	0.993	0.997	0.002	0.035	0.023
		70/30	0.999	0.998	0.995	0.012	0.018	0.027
Modifier Anderson et Pabis	[ $t < 0.35$ ]	50/50	0.995	0.996	0.998	0.007	0.046	0.029
		60/40	0.997	0.999	0.998	0.041	0.022	0.027
		70/30	0.998	0.998	0.998	0.012	0.028	0.026
	[0.35–0.63]	50/50	0.988	1.000	0.995	0.076	0.010	0.025
		60/40	0.998	0.996	0.997	0.028	0.036	0.031
		70/30	0.999	0.997	0.991	0.024	0.036	0.047
	[0.63–1]	50/50	0.996	0.996	0.999	0.010	0.042	0.021
		60/40	0.997	0.998	0.998	0.003	0.031	0.023
		70/30	0.999	0.998	0.998	0.008	0.029	0.026

Table 4 shows that the Verma et al. model better correlates with the different experimental points of the drying kinetics for the 3 isotherms. The different parameters of the model are presented in Table 5.

A representative curve of the Verma et al. model is shown in Figure 4. A strong correlation of the Verma et al. model is observed for the 3 isotherms. Considering the wet and anhydrous masses of the samples and applying equation (2), we obtain the relative humidity ratio (THR), a graph, which is shown in Figure 5. The THR (%) varies from  $5.37 \pm 0.7\%$  to  $11.65 \pm 1.4\%$ . The moisture content increases with an increase in particle size and percentage of reinforcement. This is due to the hydrophilic nature of Iroko particles. Such observations are generally observed on plant products [4, 6, 9]. The results found in this study are in line with those of Dawoua Kaoutoing et al. [9] and Betené et al., [33].

The diffusion coefficient is determined using equation (4) while the corrected diffusion coefficient is determined using equation (5). The results of the diffusion coefficients are shown in Table 6.

The results presented in Table 6 show that the corrected diffusion coefficient is lower than the diffusion coefficient. This has been observed in the literature [27]. The results obtained are greater than those found on ginger rhizomes by Ndukwu et al. [34]. The Arrhenius curve for one sample, as shown in Figure 6, is similar for all other formulations. This Arrhenius curve is obtained using corrected diffusion values. Table 7 shows the activation energy and slope values. The activation energy results obtained are lower than those for epoxy resin, which is 110 kJ/mol [35]. Epoxy resin improves the activation energy values of the composite for use in hot zones. The values obtained are close to those of oil palms [36] and spicewood [37]. The results are lower than those obtained for Nova Dubnica wood [38].

*3.1.2. Apparent and Real Density.* The curve in Figure 7 shows that the apparent density decreases with an increase in percentage and particle size. A similar finding has been observed on other composites [1, 4, 7]. This is justified by the porous nature of Iroko particles and the fact that the matrix

TABLE 5: Constancy parameters of the Verma et al. model.

Authors	Different formulations	$k$			$a$			$g$			
		90°C	80°C	70°C	90°C	80°C	70°C	90°C	80°C	70°C	
Page	[ $t < 0.35$ ]	50/50	0.240	0.145	0.004	0.293	0.421	0.042	0.041	0.038	0.064
		60/40	0.032	0.039	0.021	0.765	0.625	0.371	0.376	0.097	0.103
		70/30	0.239	0.109	0.018	0.423	0.659	0.149	0.041	0.036	0.103
	[0.35–0.63]	50/50	0.404	0.137	0.114	0.457	0.696	0.776	0.040	0.034	0.026
		60/40	0.035	0.039	0.014	0.639	0.596	0.096	0.474	0.086	0.084
		70/30	0.037	0.129	0.019	0.672	0.281	0.247	0.167	0.041	0.087
	[0.63–1]	50/50	0.031	0.150	0.096	0.416	0.523	0.878	0.444	0.039	0.018
		60/40	0.684	0.211	0.018	0.371	0.149	0.191	0.043	0.056	0.100
		70/30	0.225	0.087	0.017	0.527	0.790	0.196	0.038	0.031	0.107

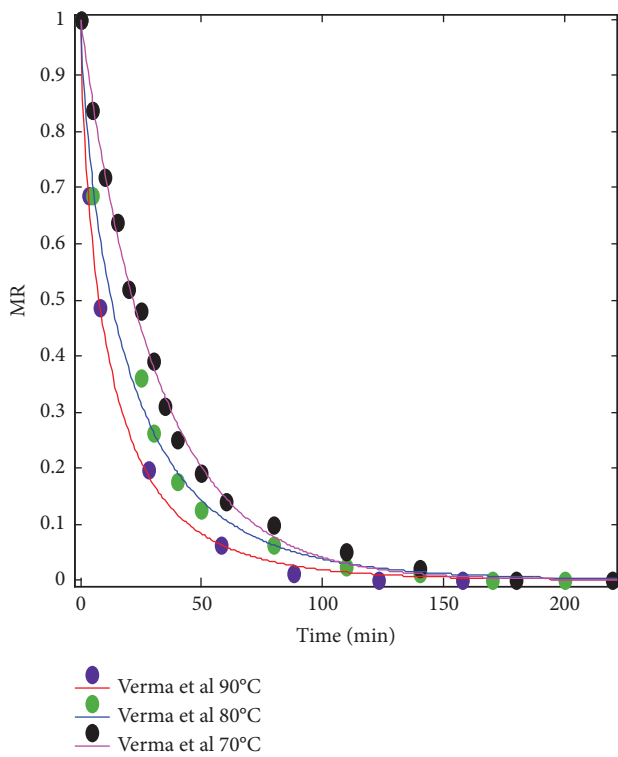


FIGURE 4: Representative curve from Verma et al.

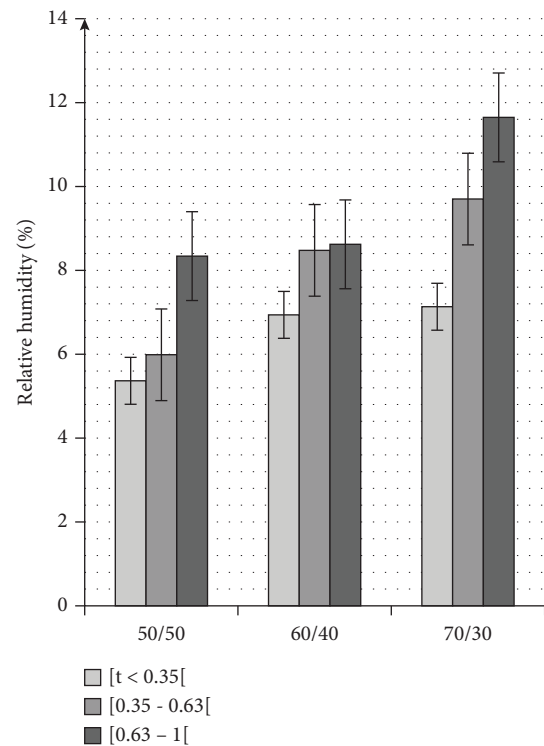


FIGURE 5: Relative humidity curve.

has a higher density than the particles. Apparent density values range from  $337.67 \pm 27.34 \text{ kg}\cdot\text{m}^{-3}$  to  $638.22 \pm 34.89 \text{ kg}\cdot\text{m}^{-3}$ . The results obtained are lower than those obtained by Huisken et al. [30], Youbi et al. [4], and Dawoua Kaoutoing et al. [9]. These results are in the same order of magnitude as those of Masri et al. [7], Mbou et al. [1], and Amadji et al. [39]. The real density (Figure 8) varies from  $444.2 \pm 40.92 \text{ kg}\cdot\text{m}^{-3}$  to  $676.81 \pm 13.59 \text{ kg}\cdot\text{m}^{-3}$ . The results obtained are lower than those for composites manufactured by Huisken et al. [30] and Youbi et al. [4], whose composites were classified as light and porous with applications in building insulation and the automobile industry.

3.1.3. Porosity Rate and Water Absorption Rate. The curve in Figure 9 shows that the rate of water absorption increases with an increase in particles and the percentage of

reinforcement. This has been observed on other composites [1, 4, 30, 39]. This increase is due to the fact that Iroko is a hydrophilic and porous wood. The porosity curve shown in Figure 10 follows the same trend as the absorption curve. Water absorption values range from  $60.96 \pm 6.26\%$  to  $168.06 \pm 11.15\%$ . The absorption results are lower than those of Iroko, which is 298% [19]. This is due to the hydrophobic nature of the epoxy matrix [4]. The porosity values ranging from 5.7% to 23.98% were found to be higher than those of Mbou et al. [1] and Kazemi et al. [40] but lower than those of Amadji et al. [39] and Youbi et al. [4].

3.1.4. Water Absorption Kinetics and Diffusion Coefficient. The curve that best correlates with the experimental points is obtained by testing the models in Table 3. The parameters obtained in the course of modeling are presented in Table 8,

TABLE 6: Diffusion coefficients of the composites produced.

Different formulations		Corrected diffusion coefficient ( $\text{m}^2 \cdot \text{s}^{-1}$ )			Diffusion coefficient ( $\text{m}^2 \cdot \text{s}^{-1}$ )		
		90°C	80°C	70°C	90°C	80°C	70°C
[ $t < 0.35$ ]	50R-50M	$1.92E-08$	$1.01E-08$	$5.31E-09$	$4.00E-08$	$2.15E-08$	$1.15E-08$
	60R-40M	$1.96E-08$	$1.26E-08$	$8.45E-09$	$4.38E-08$	$2.61E-08$	$1.83E-08$
	70R-30M	$2.16E-08$	$1.27E-08$	$5.80E-09$	$4.50E-08$	$2.77E-08$	$1.15E-08$
[0.35-0.63]	50R-50M	$3.24E-09$	$1.71E-09$	$1.06E-09$	$4.05E-09$	$2.20E-09$	$1.36E-09$
	60R-40M	$2.16E-08$	$1.11E-08$	$5.53E-09$	$4.59E-08$	$2.52E-08$	$1.16E-08$
	70R-30M	$2.85E-08$	$1.45E-08$	$6.60E-09$	$7.17E-08$	$3.26E-08$	$1.47E-08$
[0.63-1]	50R-50M	$2.54E-08$	$1.29E-08$	$7.93E-09$	$5.62E-08$	$3.08E-08$	$1.84E-08$
	60R-40M	$2.35E-08$	$1.36E-08$	$6.47E-09$	$5.57E-08$	$3.17E-08$	$1.41E-08$
	70R-30M	$2.80E-08$	$1.78E-08$	$6.39E-09$	$6.93E-08$	$4.44E-08$	$1.43E-08$

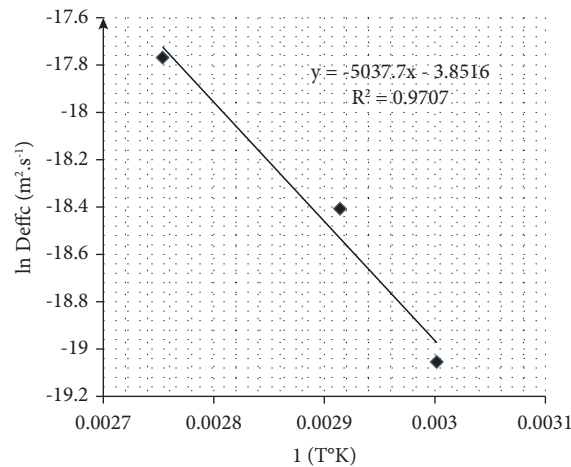


FIGURE 6: Arrhenius curve.

TABLE 7: Activation energy and Arrhenius slope

Particle size	Parameters obtained	Reinforcement rate		
		50R-50M	60R-40M	70R-30M
[ $t < 0.35$ ]	Ea (kJ/mol)	<b>41.88</b>	<b>27.54</b>	<b>42.04</b>
	Pente ( $R^2$ )	5037.7 (0.9707)	3312.1 (0.9809)	5056.1 (0.923)
[0.35-0.63]	Ea (kJ/mol)	<b>37.02</b>	<b>44.28</b>	<b>47.34</b>
	Pente ( $R^2$ )	4453.3 (0.9918)	5326.4 (0.9667)	5694.2 (0.9549)
[0.63-1]	Ea (kJ/mol)	<b>38.49</b>	<b>41.42</b>	<b>46.37</b>
	Pente ( $R^2$ )	4629.1 (0.9944)	4981.8 (0.9361)	5577.6 (0.8581)

The bold values indicate correspond to the activation energy (Ea) required.

namely, the correlation coefficients ( $R^2$ ) and the root mean square error (RMSE).

Table 8 shows that Page's model correlates best with the different experimental points obtained during the water absorption test, with a correlation of 0.99 for all formulations of the composite and a small squared error of the order of [0.008-0.026]. Figure 11 shows the curves for the different models tested, which are presented in Tables 3 and 9 showing the Page's model parameters that were obtained during the test.

Table 10 shows the diffusion results. During drying, the corrected diffusion coefficient is lower than the diffusion coefficient. The values obtained are lower than those found for raffia vinifera cork [31] and flax fiber composites [27].

**3.2. Mechanical Characterisation with the Three-Point Bending Test.** The bending test was carried out on 10 samples of each formulation, making a total of 90 samples. The test was carried out at the Mechanic and Adapted Materials Laboratory (LAMMA) in accordance with the ASTM D790 standard. At the end of the test, the force-displacement parameters for each sample were recorded. Figure 12 shows the force-displacement curve.

Figure 12 shows that the behavior of the composite varies according to the percentage of reinforcement. The higher the percentage of reinforcement, the more ductile the composite. This is justified by the fact that the epoxy matrix is brittle [4, 30]. The lower the percentage of reinforcement, the higher the maximum force. In addition, it can be said that for



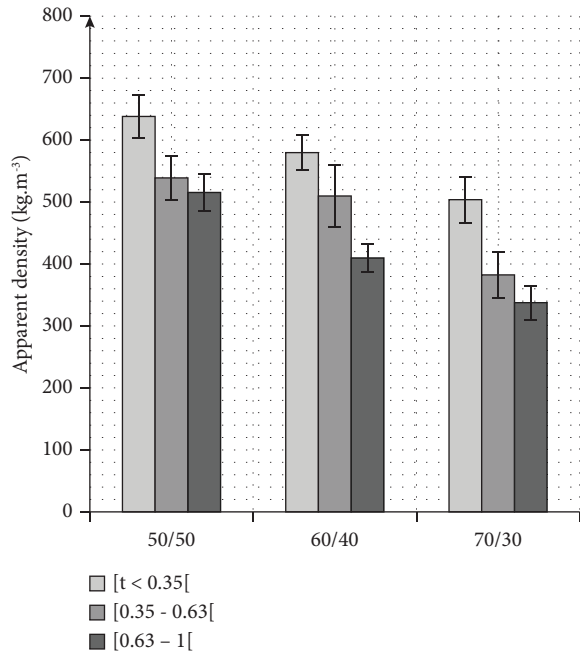


FIGURE 7: Apparent density.

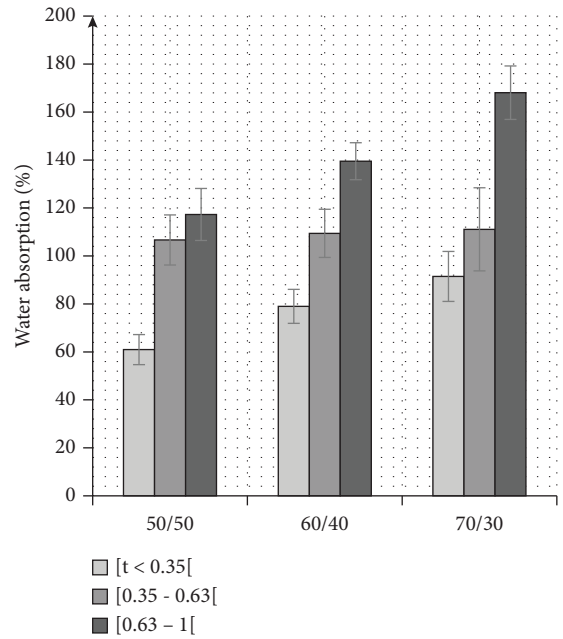


FIGURE 9: Water absorption rate curve.

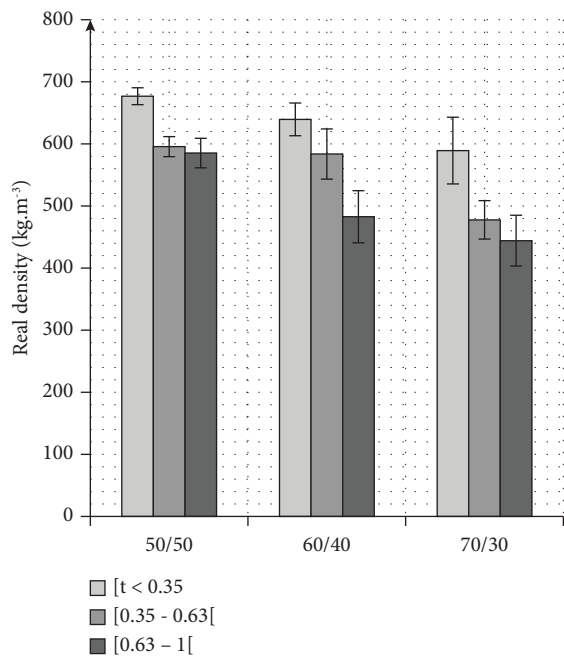


FIGURE 8: Real density.

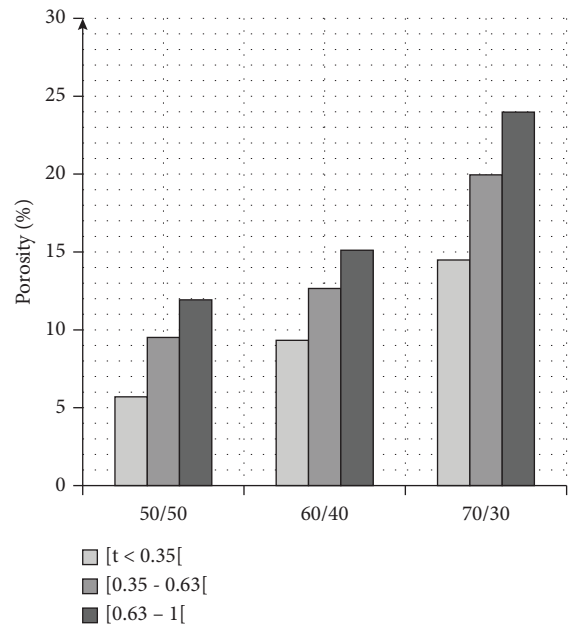


FIGURE 10: Porosity rate curve.

small reinforcement sizes, failure is progressive, unlike for large reinforcement sizes. This may justify the observations in Figure 12, which suggest that there is low wettability between the small particles and the matrix. A similar behavior has been observed by other authors [7, 41, 42]. Young's modulus curve (Figure 13(a)) decreases with an increase in the percentage of reinforcement and particle size. The same observation is made in Figure 13(b) for the stress at rupture. This makes it possible to establish a correlation between low-density values and high-water absorption and

porosity for large particles. A similar behavior has been observed in other composites [1, 43]. Young's modulus varies from  $53.21 \pm 7.13$  to  $80.25 \pm 16.57$  MPa. The stress at rupture ranged from  $0.487 \pm 0.065$  to  $4.116 \pm 0.384$  MPa. The results obtained are compared with those of other composites in Table 11.

The results obtained during various characterisations show that the composites produced are hydrophilic due to the nature of the reinforcement. In addition to this, the results show that these composites have a good diffusion capacity and are porous and lightweight, suggesting

TABLE 8: Parameters of the kinetics models.

Authors	Different formulations	$R^2$			RMSE		
		50R-50M	60R-40M	70R-30M	50R-50M	60R-40M	70R-30M
Page	$[t < 0.35[$	0.9945	0.9993	0.9959	0.0259	0.0098	0.0223
	$[0.35-0.63[$	0.998	0.9956	0.9982	0.0171	0.0262	0.0164
	$[0.63-1[$	0.999	0.9996	0.999	0.0122	0.0083	0.0114
Sikame	$[t < 0.35[$	0.9918	0.9974	0.9992	0.0328	0.0199	0.0101
	$[0.35-0.63[$	0.9982	0.9961	0.9986	0.0169	0.0256	0.0150
	$[0.63-1[$	0.9993	0.9997	0.9993	0.0110	0.0078	0.0096
Mohsenin	$[t < 0.35[$	0.9917	0.998	0.9955	0.0323	0.0169	0.0240
	$[0.35-0.63[$	0.9987	0.9952	0.9983	0.0141	0.0279	0.0164
	$[0.63-1[$	0.9988	0.9963	0.9957	0.0137	0.0248	0.0239

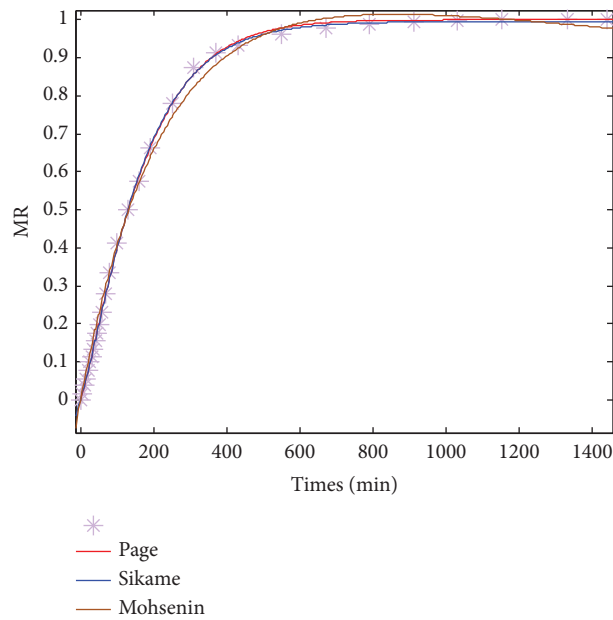


FIGURE 11: Curves of the models tested for water absorption kinetics.

TABLE 9: Page model constancy parameters.

Different formulations		$k$	$n$	$a$
$[t < 0.35[$	50-50	0.0357	0.6974	1.048
	60-40	0.0121	0.8554	1.017
	70-30	0.0345	0.6756	1.062
$[0.35-0.63[$	50-50	0.0096	0.9465	1.012
	60-40	0.0060	0.9929	1.023
	70-30	0.0082	0.9702	1.019
$[0.63-1[$	50-50	0.0070	0.9829	1.019
	60-40	0.0021	1.1900	0.9982
	70-30	0.0211	0.8087	1.016

TABLE 10: Different diffusion coefficients

Different formulations	Corrected diffusion coefficient ( $m^2 \cdot s^{-1}$ )			Diffusion coefficient ( $m^2 \cdot s^{-1}$ )		
	50R-50M	60R-40M	70R-30M	50R-50M	60R-40M	70R-30M
$[t < 0.35[$	$1.59E-09$	$1.52E-09$	$1.28E-09$	$3.77E-09$	$3.46E-09$	$2.61E-09$
$[0.35-0.63[$	$1.51E-09$	$8.78E-10$	$1.13E-09$	$3.57E-09$	$1.73E-09$	$2.36E-09$
$[0.63-1[$	$1.23E-09$	$1.31E-09$	$1.42E-09$	$2.68E-09$	$2.69E-09$	$3.08E-09$

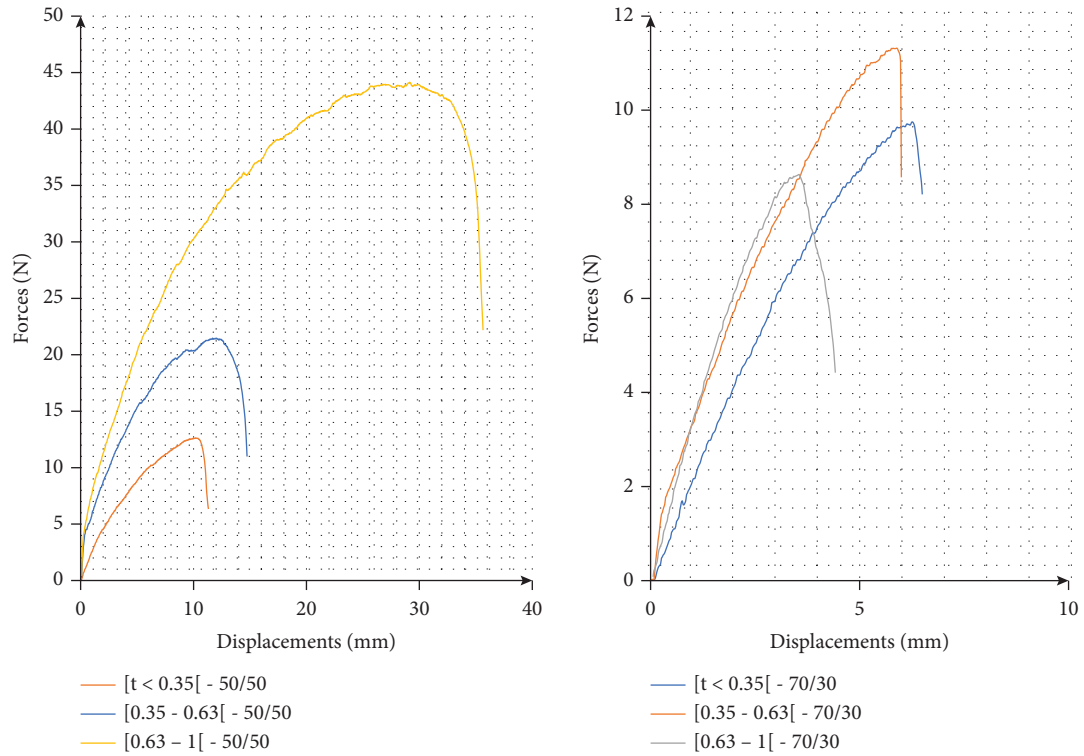


FIGURE 12: Force-displacement curve for bending test.

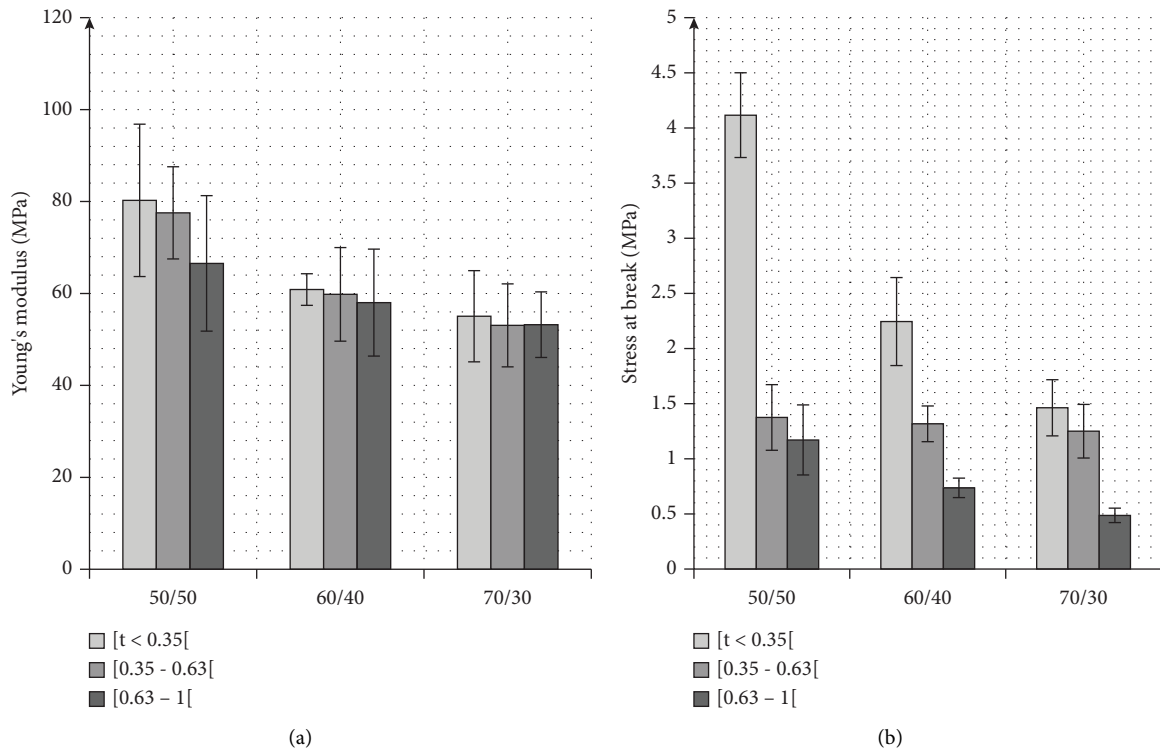


FIGURE 13: Distribution curve: (a) Young's modulus; (b) stress at break.

TABLE 11: Comparison of results with other composite materials.

Materials	Water absorption (%)	Apparent density ( $\text{kg}\cdot\text{m}^{-3}$ )	Young's modulus (MPa)	References
Raphia <i>vinifera</i> (RV)/urea (UF)	54–94	379–650	0.07–0.252	[1]
Bambusa <i>vulgaris</i> /BV/UF	56–66	471–630	0.07–0.155	
RV–BV/UF	59–87	455–629	0.07–0.286	
Date palm particle/polystyrene (PS)	—	542–824	0.12–0.76	[7]
Gmelina wood/PS	—	758.68	0.60–2.26	[39]
Rapeseed stalk	90.4	684	1798	[44]
Wood/tobacco/UF	77–124	750	438–1866	[45]
Iroko wood composite with epoxy matrix	60.96–168.06	337.67–638.22	53.21–80.25	Case studies

applications in the construction industry, furniture, thermal insulation of houses, and the automobile industry. These composites can be classified as type 2 lightweight according to the EN312 standard. These materials can be used in both dry and wet environments [1, 9, 33].

#### 4. Conclusion

The aim of this work was to produce composites using sawdust waste from Iroko *Chlorophora excelsa*. In this work, several parameters were explored, including the percentage of reinforcement (Iroko particles) and particle size. A set of sieves was used to distinguish 3 particle sizes ( $[t < 0.35]$ ,  $[0.35–0.63]$ , and  $[0.63–1]$ ). Three reinforcement percentages were used (50R/50M, 60R/40M, and 70R/30M). Molding was carried out under cold pressure as described by Mbou et al. to obtain samples measuring  $180 * 180 * 10 \pm 1$  mm. Physical tests were carried out using the gravimetric method: apparent and real density, porosity, desorption cycle, and water absorption. A three-point bending test based on the principle of the ASTM D790 standard was carried out to determine the mechanical characteristics of the composite. The physical results showed that incorporating the particles into the matrix lightened the material, while also making it more absorbent and porous. The results obtained can be compared to those of other composites and lightweight woods used for insulation and construction. The bending results are in the same order of magnitude as those of lightweight woods used in construction and insulation. It has been observed that absorption and porosity increased while mechanical characteristics (Young's modulus and mechanical strength) and density decreased with an increase in particle size and percentage of reinforcement. The results obtained were compared with those of other materials in the literature whose applications were defined. The applications of the composites produced will be oriented in the same direction. The results obtained make it possible to classify the material as lightweight type 2, which is suitable for use in dry and damp areas in accordance with the EN312 standard for any given formulation. The authors recommend that thermal conductivity be determined by thermal testing, and that chemical (ATG, FTIR, and XRD), microstructural (SEM), and durability analyses be carried out to define other areas of application. The authors recommend optimizing the molding process by applying chemical treatments to the particles before making other composite materials.

#### Data Availability

The data used to support the findings of this study have not been the subject of any prior study.

#### Conflicts of Interest

The authors declare that they have no conflicts of interest.

#### Acknowledgments

The authors would like to thank Mr Ebenezer Njeugna, head of Mechanics and Adapted Materials Laboratory (LAMMA), and Mr Alphonse Tchoukouabe, head of maintenance at the Laboratory of Génie Civile, ENSET, Douala, for making the physical and mechanical test equipment available. The authors would also like to thank Mr. Christian Roi Taneke Ananbe for his help in analysing the results.

#### References

- [1] E. Mbou Tiaya, P. W. Huisken Mejouyou, P. A. Ndema Ewane, C. Damfeu, P. Meukam, and E. Njeugna, "Effect of particle sizes on physical, thermal and mechanical behavior of a hybrid composite with polymer matrix with raffia vinifera cork and Bambusa vulgaris," *Polymer Bulletin*, vol. 81, no. 1, pp. 275–295, 2023.
- [2] C. Takoumbe, E. M. Tiaya, D. Ndapeu et al., "Selected physical and mechanical properties of the oil palm pseudo-trunk: case of the Tenera variety from Cameroon," *Results in Materials*, vol. 17, Article ID 100354, 2023.
- [3] N. Defo, R. N. T. Sikame, W. P. M. Huisken et al., "Development and characterization of agglomerated abrasives based on agro-industrial by-products," *Journal of Natural Fibers*, vol. 20, no. 1, 2023.
- [4] S. B. T. Youbi, O. Harzallah, N. R. S. Tagne et al., "«Effect of Raphia vinifera fibre size and reinforcement ratio on the physical and mechanical properties of an epoxy matrix composite: micromechanical modelling and weibull analysis," *International Journal of Polymer Science*, vol. 2023, Article ID 5591108, 20 pages, 2023.
- [5] S. B. T. Youbi, N. R. S. Tagne, O. Harzallah et al., "«Effect of alkali and silane treatments on the surface energy and mechanical performances of Raphia vinifera fibres," *Industrial Crops and Products*, vol. 190, Article ID 115854, 2022.
- [6] A. B. N. Deugoué, N. R. T. Sikame, P. W. M. Huisken, G. Tchemou, S. T. Tiwa, and E. Njeugna, "Banana–plantain fiber limited life geotextiles (PFLLGs): design and

- characterization,” *Indian Geotechnical Journal*, vol. 53, no. 4, pp. 874–886, 2023.
- [7] T. Masri, H. Ounis, L. Sedira, A. Kaci, and A. Benchabane, “Characterization of new composite material based on date palm leaflets and expanded polystyrene wastes,” *Construction and Building Materials*, vol. 164, pp. 410–418, 2018.
- [8] A. D. Betené Omgba, J. C. Obam, S. Youssoufa et al., “Effect of extension speed on the mechanical performance of sisal and coir fiber bundles,” *International Journal of Polymer Analysis and Characterization*, vol. 29, no. 2, pp. 86–97, 2024.
- [9] M. Dawoua Kaoutoing, B. Ndiwe, L. Karga et al., “Characterisation of a composite material with polyester matrix reinforced with particles from doum palm (hyphaene thebaica) fruit,” *Results in Materials*, vol. 18, Article ID 100401, 2023.
- [10] N. P. Bakehe, “L’effet de l’exposition au bois de chauffage sur la santé respiratoire et sur la participation au marché du travail au Cameroun,” *Revue Française d’Economie*, vol. 36, no. 2, pp. 163–195, 2021.
- [11] W. T. Tomen, B. S. Diboma, B. V. Bot, and J. G. Tamba, “Physical and Combustion properties investigation of hybrid briquettes from tropical Sawdust: case study of Iroko (*Milicia excelsa*) and Padouk (*Pterocarpus soyauxii*),” *Energy Reports*, vol. 9, pp. 3177–3191, 2023.
- [12] U. Nzotcha and J. Kenfack, “Contribution of the wood-processing industry for sustainable power generation: viability of biomass-fuelled cogeneration in Sub-Saharan Africa,” *Biomass and Bioenergy*, vol. 120, pp. 324–331, 2019.
- [13] J. Z. Mfomo, A. B. Biwolé, E. Fedoung Fongzossie et al., “Carbonization techniques and wood species influence quality attributes of charcoals produced from industrial sawmill residues in Eastern Cameroon,” *Bois et Forêts des Tropiques*, vol. 345, pp. 65–74, 2020.
- [14] D. G. Christelle, N. C. Elvis, N. K. Clovis et al., “Biosciences and plant biology,” *Int. J. Curr. Res. Biosci. Plant Biol*, vol. 7, no. 9, pp. 1–9, 2020.
- [15] C. Cunha, M. Tenório, D. F. Lima, A. Rebouças, L. C. Neves, and J. M. Branco, “Mechanical characterization of Iroko wood using small specimens,” *Buildings*, vol. 11, no. 3, p. 116, 2021.
- [16] A. C. Njamen, A. Kemajou, and L. Monkam, “Experimental study of the thermal behaviour of a building with an Iroko wood envelope in the city of Douala, Cameroon,” *Journal of Renewable Energies*, vol. 21, no. 2, 2018.
- [17] D. Kačíková, I. Kubovský, N. Ulbriková, and F. Kačík, “The impact of thermal treatment on structural changes of teak and Iroko wood lignins,” *Applied Sciences*, vol. 10, no. 14, p. 5021, 2020.
- [18] M. Simo-Tagne, A. Zoulalian, R. Remond, Y. Rogaume, and B. Bonoma, “Modeling and simulation of an industrial indirect solar dryer for Iroko wood (*Chlorophora excelsa*) in a tropical environment,” *Maderas: Ciencia y Tecnología*, vol. 19, no. ahead, p. 112, 2017.
- [19] S. K. Papy and N. Timothée, “Study of physical and mechanical properties of wood concrete,” *OALib*, vol. 10, no. 1, pp. 1–11, 2023.
- [20] G. Todou, M. Hassan, A. Ze, D. Kombo, S. Machewere, and T. Vroumsia, “Diversity of used plant species for producing charcoal and its trade-off in Far-North Region, Cameroon,” *International Journal of Environmental Research and Public Health*, vol. 6, no. 2, pp. 19–29, 2017.
- [21] H. Kouakou, A. C. Djohore, and E. Emeruwa, “Influence of cassava starch content on the quality of a biochar based on sawdust and cassava starch,” *Boichar*, vol. 5, 2019.
- [22] J. J. E. Biwolé, A. B. Biwolé, A. Pizzi et al., “A review of the advances made in improving the durability of welded wood against water in light of the results of african tropical woods welding,” *Journal of renewable materials*, vol. 11, p. 23, 2022.
- [23] H. Bouafif, A. Koubaa, P. Perré, et al., A. Cloutier, “Effects of fiber characteristics on the physical and mechanical properties of wood plastic composites,” *Composites Part A: Applied Science and Manufacturing*, vol. 40, no. 12, pp. 1975–1981, 2009.
- [24] S. Migneault, A. Koubaa, F. Erchiqui, A. Chaala, K. Englund, et al., M. P. Wolcott, “Effects of processing method and fiber size on the structure and properties of wood-plastic composites,” *Composites Part A: Applied Science and Manufacturing*, vol. 40, no. 1, pp. 80–85, 2009.
- [25] S. K. Kana, A. B. Biwolé, P. W. Mejouyo Huisken et al., “Physical and mechanical properties of two tropical wood (*Detarium macrocarpum* and *Piptadeniastrum africanum*) and their potential as substitutes to traditionally used wood in Cameroon,” *International Wood Products Journal*, 2024.
- [26] P. W. Huisken Mejouyo, E. M. Tiaya, N. R. Sikame Tagne, S. T. Tiwa, and E. Njeugna, “Experimental study of water sorption and desorption of several varieties of oil palm mesocarp fibers,” *Results in Materials*, vol. 14, Article ID 100284, 2022.
- [27] D. Scida, M. Assarar, A. Rezak, and C. Poilâne, “Effect of Moisture on the Mechanical Behaviour of Flax Fibre Composites,” 2011.
- [28] D. Ndapeu, E. Njeugna, N. R. Sikame, S. B. Bistac, J. Y. Drean, and M. Fogue, “Experimental study of the water absorption kinetics of the coconut shells (*nucifera*) of cameroun,” *Materials Sciences and Applications*, vol. 7, no. 3, pp. 159–170, 2016.
- [29] K. Schössler, H. Jäger, and D. Knorr, “Effect of continuous and intermittent ultrasound on drying time and effective diffusivity during convective drying of apple and red bell pepper,” *Journal of Food Engineering*, vol. 108, no. 1, pp. 103–110, 2012.
- [30] P. W. M. Huisken, G. Tchémou, N. R. S. Tagne, D. Ndapeu, et al., E. Njeugna, “Effect of the addition of oil palm mesocarp fibers on the physical and mechanical properties of a polyester matrix composite,” *International Journal of Polymer Science*, vol. 2022, Article ID 3399986, 12 pages, 2022.
- [31] E. T. Mbou, E. Njeugna, A. Kemajou, N. R. T. Sikame, and D. Ndapeu, “Modelling of the water absorption kinetics and determination of the water diffusion coefficient in the pith of raffia *vinifera* of bandjoun, Cameroon,” *Advances in Materials Science and Engineering*, vol. 2017, pp. 1–12, 2017.
- [32] S. M. Anafack, O. Harzallah, D. E. Nkemaja et al., “Effects of extraction techniques on textile properties of William banana peduncle fibers,” *Industrial Crops and Products*, vol. 201, 2023.
- [33] A. D. O. Betené, B. Ndiwe, G. S. Krishnan et al., “Processing of tropical agro-industrial waste for particleboard manufacture: dimensional stability and mechanical performance,” *Journal of Building Engineering*, vol. 76, Article ID 107369, 2023.
- [34] M. C. Ndukwu, E. B. Augustine, E. Ugwu et al., “Drying kinetics and thermo-economic analysis of drying hot water blanched ginger rhizomes in a hybrid composite solar dryer with heat exchanger,” *Heliyon*, vol. 9, no. 2, Article ID e13606, 2023.
- [35] A. Cherdoud-Chihani, M. Mouzali, and M. J. Abadie, “Parametres cinetiques de systemes epoxy/acide par analyse calorimetrique differentielle (DSC),” *Journal of Thermal Analysis and Calorimetry*, vol. 70, no. 2, pp. 527–540, 2002.

- [36] J. Guo and A. C. Lua, “Kinetic study on pyrolytic process of oil-palm solid waste using two-step consecutive reaction model,” *Biomass and Bioenergy*, vol. 20, no. 3, pp. 223–233, 2001.
- [37] J. Martinka, V. Mózer, E. Hroncová, and J. Ladomerský, “Influence of spruce wood form on ignition activation energy,” *Wood Research*, vol. 60, 2015.
- [38] L. Gašparovič, J. Labovský, J. Markoš, and L. Jelemenský, “Calculation of kinetic parameters of the thermal decomposition of wood by distributed activation energy model (DAEM),” *Chemical and Biochemical Engineering Quarterly*, vol. 26, 2012.
- [39] T. A. Amadji, E. C. Adjovi, J. Gérard, J. Barés, and V. Huon, “Étude des propriétés technologiques d’un composite bois-plastique élaboré au Bénin,” *Bois et Forêts des Tropiques*, vol. 348, pp. 49–63, 2021.
- [40] S. K. Najafi, A. Kiaefar, E. Hamidina, and M. Tajvidi, “Water absorption behavior of composites from sawdust and recycled plastics,” *Journal of Reinforced Plastics and Composites*, vol. 26, no. 3, pp. 341–348, 2007.
- [41] M. A. Binhussain and M. M. El-Tonsy, “Palm leave and plastic waste wood composite for out-door structures,” *Construction and Building Materials*, vol. 47, pp. 1431–1435, 2013.
- [42] M. C. N. Yemele, A. Koubaa, A. Cloutier, P. Soulounganga, and M. Wolcott, “Effect of bark fiber content and size on the mechanical properties of bark/HDPE composites,” *Composites Part A: Applied Science and Manufacturing*, vol. 41, no. 1, pp. 131–137, 2010.
- [43] A. C. De Almeida, V. A. De Araujo, E. A. M. Morales et al., “Wood-bamboo particleboard: mechanical properties,” *Bio-resources*, vol. 12, no. 4, pp. 7784–7792, 2017.
- [44] A. B. Akinyemi, J. O. Afolayan, and E. Ogunji Oluwatobi, “Some properties of composite corn cob and sawdust particle boards,” *Construction and Building Materials*, vol. 127, pp. 436–441, 2016.
- [45] Y.-S. Oh and M. A. Jamaludin, “Avaliação de caule da colza aglomerado vinculado com laboratório resina ureia-formaldeído,” *Ciência Florestal*, vol. 25, no. 2, pp. 515–521, 2015.